Cellulose gelation in aqueous hydroxide solutions by CO<inf>2</inf>(g): Fact and theory

Carbohydrate Polymer Technologies and Applications 7 (2024) 100514

Contents lists available at ScienceDirect

Carbohydrate Polymer Technologies and Applications

journal homepage: www.sciencedirect.com/journal/carbohydrate-polymer-technologies-and-applications

Cellulose gelation in aqueous hydroxide solutions by CO_2(g): Fact and theory

Shirin Naserifar [a,b,*], Nabin Kumar Karna [c], Aleksandra Maria Kozlowski [d], Diana Bernin [a], Merima Hasani [a,b]

[a] Department of Chemistry and Chemical Engineering, Chalmers University of Technology, 41296 Gothenburg, Sweden
[b] Wallenberg Wood Science Center, Chalmers University of technology, 41296 Gothenburg, Sweden
[c] Tree to Textile, 43153 Mölndal, Sweden
[d] RISE Research Institutes of Sweden, 43153 Mölndal, Sweden

ARTICLE INFO

Keywords:
Cellulose
Gelation
Quaternary ammonium hydroxide
CO_2(g), MD simulations

ABSTRACT

Understanding how the solvent structure affects the stability of the dissolved state and the following precipitation is important for designing future dissolution-coagulation systems for cellulose processing. In this study, two morpholinium hydroxides with different alkyl chain lengths, namely *N,N*-dimethylmorpholinium hydroxide (NDMMOH(aq)) and *N*-butyl-*N*-methyl morpholinium hydroxide (BMMorOH(aq)), were studied and compared with the previously thoroughly investigated cellulose solvent benzyltriemethylammonium hydroxide (Triton B (aq)) which is well-known for its superior ability to stabilize the dissolved state. Cellulose solutions in each solvent were characterized by NMR, flow and frequency sweeps, while cellulose coagulation by CO_2(g) was followed by in situ FTIR, pH and temperature measurements. The coagulated systems were characterized by CP/MAS ^{13}C NMR, flow, and frequency sweep measurements. Complementary molecular dynamic (MD) simulations were performed to gain a deeper insight into the observed gelation behavior. The intrinsic viscosity indicated more extended cellulose chains in the solvents with more hydrophobic moieties (Triton B and BMMorOH). Even though the course of coagulation did not show any significant differences during monitoring, both the properties of the obtained gels and the MD simulations indicated differences in formation and properties of the coagulated materials that could be related both to the choice of solvent and coagulant.

1. Introduction

In the urgent shift towards renewable resources due to pollution and rapid global warming, cellulose being the most available biopolymer has attracted significant attention since it can be used in a wide range of material applications. Cellulose dissolution and regeneration are usually required for some of the applications. However, the inability of cellulose to dissolve (a prerequisite step before regeneration) or melt (for its further processing) remains a challenge to overcome. Cellulose is an amphiphilic polymer composed of glucose units connected via 1,4-glycosidic linkages (O'sullivan, 1997). Its amphiphilicity stems from the equatorial position of its hydroxyl groups (creating hydrophilic regions on the edges of the pyranose rings and allowing for inter-and intramolecular hydrogen bonding), in contrast to the solely axially positioned C—H groups creating hydrophobic areas parallel to the pyranose ring plane. As a consequence, adjacent chains are assembled in an extended sheet framework through hydrogen bonding, with hydrophobic areas extending above and below the pyranose ring planes promoting further stacking into a crystalline structure via van der Waals interactions (Medronho & Lindman, 2015) and water exclusion. This complex structure is, as such, resistant to dissolution, thus solvent capable of overcoming a combined effect of these interactions is required to aid cellulose processing. Besides, a choice of a coagulating agent for cellulose processing is just as critical. Over time, different solvents have been introduced and investigated either as derivatizing solvents in which cellulose is transformed into a soluble derivative or direct solvents in which intermolecular interactions between the solvent and cellulose lead to dissolution. CS_2/NaOH(aq) (Cross et al., 1982; Donald & Reginald, 1951) and *N*-methyl morpholinium-*N*-oxide (NMMO) monohydrate (Clarence & McCorsley, 1981) are examples of derivatizing and non-derivatizing solvents which have been utilized industrially in viscose and lyocell process, respectively. In addition,

* Corresponding author.
E-mail address: shirin.naserifar@chalmers.se (S. Naserifar).

https://doi.org/10.1016/j.carpta.2024.100514

Available online 15 May 2024

multitude number of direct solvents have been developed for analytical work as well as chemical modifications of cellulose and dissolution-coagulation processing., namely, alkali containing solvents e.g. NaOH(aq)/urea (Olsson & Westman, 2013), dimethylacetamide/-lithium chloride (DMAc/LiCl) (Mccormick et al., 1985), phosphoric acid (Boerstoel et al., 2001), dimethyl sulfoxide/tetrabutylammonium fluoride (DMSO/TBAF) (Liebert & Heinze, 2001), ionic liquids (Zhu et al., 2006) and quaternary ammonium hydroxides (Kostag et al., 2018). Yet, low dissolution capacity, side reactions under required dissolution conditions and cellulose degradation are examples of set-backs which arise the need to actively develop new solvents for cellulose. Moreover, understanding of how the structural features of solvent affect the coagulation process and the properties of the coagulated material is scarce.

In this regard, quaternary ammonium hydroxides (QAHs) have been investigated for their ability to dissolve cellulose since 1924 (Lilienfeld, 1930). These groups of solvents are of particular interest mainly because of their easy synthesis and water as their major constituent. Tetrabutylammonium hydroxide (TBAH) (Gubitosi et al., 2016), tetramethylammonium hydroxide (TMAH) (Zhong et al., 2015), triethylmethyl ammonium hydroxide, tetraethylammonium hydroxide (TEAH) and benzyltriemethylammonium hydroxide (Triton B) (Wang et al., 2018), dimethyldibenzylammonium hydroxide (Triton F) and tetrabutylammonium hydroxide (TBAH) (Wei et al., 2015), are some examples. The latter two, i.e.: the benzyl-substituted QAHs have proven to be very efficient solvents due to the bulkiness of the cations which enhances disruption of cellulose-cellulose stabilizing interactions (Ehert & Lieser, 1937; Powers & Bock, 1935). Recently, our group has developed a series of morpholinium-based solvents (inspired by industrially used NMMO) and investigated the impact of their structural properties on cellulose dissolution (Naserifar et al., 2021, 2023). Following up on that work additional knowledge is needed on the importance of structural motifs of the solvent, specifically the impact of the cation structure (in the case of aqueous hydroxides) on cellulose dissolved state. When it comes to cellulose coagulation and the characteristics of the coagulated material, the impact of solvent cation structure is even less known. Based on previous investigations of cellulose in hydroxide solutions, both the level of deprotonation and ability of the solvent to stabilize the hydrophobic regions of cellulose are likely affected by the structural motifs of the cation. On the other hand, introduction of the structure-making carbonate (CO_3^{2-}) is expected to enhance the cellulose-cellulose interactions through water exclusion from the regions parallel to the pyranose ring planes (accommodating the C—H structures) even further by increasing the cohesiveness of the alkaline solution. For this reason the response of different cellulose solutions to CO_2-coagulations is expected to reflect the ability of the different cations to provide stabilization against hydrophobic pairing.

In this study we have focused on two of our recently developed morpholinium hydroxide solvents (Naserifar et al., 2021, 2023) offering a structural variation with regard to the length of the alkyl chain, i.e.: *N, N*-dimethylmorpholinium hydroxide (NDMMOH) carrying a methyl group, and *N*-butyl-*N*-methylmorpholinium hydroxide (BMMorOH) carrying a butyl chain. These were compared with the structurally different benzyltriemethylammonium hydroxide (Triton B) which is well-known for its superior ability to stabilize the dissolved state (Scheme 1) compared to e.g. NaOH(aq) (Brownsett & Clibbens, 1941).

In this work we hypothesize that cation in aqueous alkaline solvents critically affect coagulation of cellulose, mainly the properties of the systems after gelation as well as the coagulated cellulose. While comparing behavior and stability of cellulose solutions, two phenomena have been of particular interest to shed light on: deprotonation and the ability to stabilize the cellulose-cellulose association (likely through hydrophobic pairing). The former has been primarily investigated by ^{1}H and ^{13}C NMR measurements, capable of detecting displacement of chemical shifts as a consequence of enhanced deprotonation and/or polar interactions while the latter has been studied by assessing the rheology of the cellulose solutions and their response to the CO_2-coagulation. In addition, intrinsic viscosity, steady shear and frequency sweep measurements on cellulose solutions have been carried out while the coagulation process has been *in line* studied by FTIR, pH and temperature measurements.

2. Materials and methods

2.1. Materials

Microcrystalline cellulose (MCC, Avicel PH-101) with particle size of ~50 μm and degree of polymerization of ~230, was purchased from Sigma-Aldrich. methyl-α-D-glucopyranoside, benzyltrimethylammonium hydroxide 40 wt% in H_2O (Triton B), *N*-methylmorpholine, bromomethane, 1-bromobutane, diethyl ether, ethyl acetate, acetonitrile and ethanol were provided from Merck. Silver(I) oxide was purchased from Alfa Aeser. CO_2(g) 99 % was provided by Linde (Gothenburg, Sweden). All the reagents were used as received without further purification and deionized water was used in all the experiments.

2.2. Synthesis of N,N-dimethylmorpholinium iodide (NDMMI)

In general, quaternary ammonium hydroxides are synthesized via alkylation of the amine followed by an ion exchange using silver(I) oxide in water (Ginsburg, 1967).

0.18 mol *N*-methylmorpholine (19.79 ml) was added to 120 ml acetonitrile. Since the methylation of *N*-methylmorpholine is exothermic, the solution was placed in an ice bath followed by dropwise addition of 0.18 mol iodomethane (11.20 ml). After a few minutes of stirring the solution in the ice bath, white precipitates appeared. To ensure complete product formation, the reaction mixture was stirred for an additional 1 h. The resulting product was then purified and isolated by adding diethyl ether to ensure complete removal of the impurities/side products formed during the reaction. Finally, the obtained precipitates were dried at ambient temperature. Yield: 87 %

2.3. Synthesis of N-butyl-N-methyl morpholinium bromide (BMMorBr)

To 0.2 mol *N*-methylmorpholine (22.05 ml), 0.25 mol 1-bromobutane (26.9 ml) and 120 ml acetonitrile were added in a round bottom flask. The reaction mixture was stirred at 70 °C for 24 h under reflux to cool down the produced vapors and avoid loss of chemicals as a result of evaporation over time. Some precipitates were formed by the end of the reaction, yet to allow full crystallization of the product, the solution was stored in a freezer at −18 °C for 1 h. Next, ethyl acetate was added to the solution promoting complete diffusion of products out of the solution.

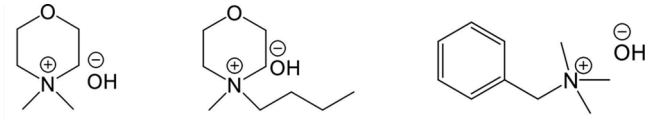

Scheme 1. The structure of the studied solvents.

Lastly, the precipitates were filtered, washed with ethyl acetate three times and dried in a vacuum oven at 50 °C for 24 h. A desiccator was used to store the dry product to avoid any moisture uptake from atmosphere. Yield: 89 %

2.4. NDMMOH(aq)/ BMMorOH(aq) synthesis

20 ml deionized water was added to 0.06 mol of NDMMI/ BMMorBr in a 45 ml centrifuge vial and the mixture was stirred to full dissolution. Next, 0.04 mol of silver(I) oxide (9.26 g) was added to the solution while stirring and the vial was sealed tightly to avoid further contact with air. As soon as silver(I) oxide was added, yellow precipitates of silver iodide were formed while by the end of the reaction, the excess grey silver(I) oxide remained unreacted. Stirring of the reaction mixture continued for approx. 5 h at room temperature. Finally, the obtained solution was centrifuged, and the supernatant containing the desired hydroxide solution was isolated and kept refrigerated. Yield: 90 %

2.5. Determination of NDMMOH(aq)/ BMMorOH(aq) concentration

An SI analytics autotitrator was used for the titration of the solutions. 1 ml of the solvent was diluted with 30 ml of deionized water and titrated against 1 M HCl. The titrant volume at the equivalence point was used to calculate the concentration of the solvent.

2.6. Cellulose dissolution

For this study the solvent concentrationwas set to 1.5 M and cellulose was added to the final concentration of 2 wt% to ensure complete cellulose dissolution.

2.6.1. Dissolution in Triton B(aq)

1.5 M Triton B(aq) was prepared by dilution of its concentrated solvent (40 wt%) with water. The solution was kept in a freezer at −25 °C to cool down. Next, MCC was added to the cold solution in an ice bath to the final concentration of 2 wt% and the solution was stirred extensively until a semi-transparent solution was obtained. The resulting solution was kept in a freezer at −25 °C for 20 min and thawed afterwards to yield a transparent solution with no undissolved cellulose detected by microscopy.

2.6.2. Dissolution in NDMMOH(aq)/ BMMorOH(aq)

1.5 M NDMMOH(aq)/BMMorOH(aq) solution was prepared by dilution of their concentrated form with water. MCC was added to the solvent to reach the final concentration of 2 wt% and the suspension was stirred at room temperature for 5 min. Next, the mixture was kept in a freezer at −25 °C for 20 min and thawed afterwards to yield a completely transparent solution.

2.7. Monitoring of coagulation

The coagulation of cellulose solutions during addition of CO_2(g) was in situ followed with FTIR and the pH and temperature variations were in line monitored.

A Mettler Toledo ReactIR 15 DiComp probe comprising of a silver halide 6 mm × 1.5 m fiber with an integrated attenuated total reference (ATR) gold sealed diamond tip was used for continuous *in line* monitoring of the reaction *via* in situ spectroscopy. Spectra are measured in an optical range of 650–3000 cm^{-1} excluding diamond region as blind spot (1950–2250 cm^{-1}). A PC was connected to the equipment with installed iC IR™ 7.1 software in which the collected results were displayed continuously with the possibility of further spectra handling and analysis. The equipment was configured to collect spectra at the resolution of eight wavenumber by averaging 79 scans in 30 second intervals until no further changes were observed in the spectra. The air background was collected prior to each run. Analysis of the gathered spectra was carried out by selection of the diagnostic peaks both manually and *via* component suggestion function of the iCIR™ 7.1 software.

A Eutech pH electrode (ECFG7451901B) and a temperature probe (PHWPTEM01W) connected to a laboratory multimeter (Eutech pH 450) were used and the pH and temperature values were collected every 30 s.

30 ml of 1.5 M desired solvent was placed in a beaker with ReactIR, pH and temperature probes inside for real time monitoring. While the solution was stirred at 850 rpm, CO_2(g) was bubbled through the mixture with flow rate of 200 ml/min through a glass inlet with a PTFE tip (∅ = 0.86 mm), secured by an overflow tube and a valve (Methrom AG, Herisau, Switzerland). During the measuring, any movement of the probes was avoided. The same procedure was followed when solutions comprising 2 wt% MCC in 1.5 M solvent were studied.

2.8. Computational method

For details on the methods used for the simulation studies, the readers are referred to the supplementary information.

2.9. Intrinsic viscosity measurements

Intrinsic viscosity measurements were measured in 1.5 M pure solvents as well as cellulose solutions in different solvents which were prepared in the concentration range 0.15–0.5 wt% according to the methods mentioned above in the dissolution section. All the solutions were kept in a water bath at 25 °C for 30 min after preparation. Viscosity measurements were carried out using a capillary viscometer equipped with circulating water bath to maintain the temperature at 25 °C, and the time (t) taken for the solutions to pass down the timing marks in the capillary was recorded. Each measurement was run in triplicate and the average measured time was used in the relative viscosity calculations. Finally, the specific viscosity (η_{sp}) was calculated using Eq. (2), and η_{sp} /C (dL/g) was plotted vs. C (g/dL) (C is the concentration). The intrinsic viscosity was obtained from linear regression, with a coefficient of determination of at least 0.97.

$$\eta_{rel} = t_{solution}/t_{solvent} \quad (1)$$

$$\eta_{sp} = \eta_{rel} - 1 \quad (2)$$

2.10. ^{1}H and ^{13}C NMR of cellulose solutions

NMR experiments were carried out on an 800 MHz (^{1}H) magnet with a TXO probe and Bruker Avance HDIII console at 298 K. ^{1}H NMR spectra were recorded using the pulse sequence zg30 and a repetition delay of 5 s and the signal was accumulated for 16 times. ^{13}C NMR spectra were recorded using a z-restored spin echo sequence (Xia et al., 2008) to avoid a rolling baseline and 64 signal accumulations.

2.11. Cross-Polarization magic-angle-spinning ^{13}C NMR (CP/MAS ^{13}C NMR)

Regenerated cellulose was subjected to solid-state NMR experiments carried out on a Bruker Avance III 500 MHz spectrometer equipped with a 4 mm HX CP MAS probe. Experiments were recorded at a magic angle spinning (MAS) rate of 10 kHz and the temperature was set to 298 K. 1H decoupling with a "spinal64'' decoupling scheme at 67 kHz was applied during the acquisition. The cross-polarization (CP) contact time was set to 1.5 ms and the repetition time to 2 s. CP spectra for comparison were recorded with 4000 signal accumulations.

2.12. Flow sweep measurements

Flow sweep measurements of cellulose solutions in different solvents at 23 °C and shear rates of 1–100 1/s were measured using a TA Discovery Hybrid Rheometer (HR-3), with a sandblasted 40-mm plate-plate

geometry with a gap of 500 μm when using Triton B and 400 μm when using NDMMOH(aq) or BMMorOH(aq). A water filled solvent trap was used to avoid solvent evaporation while running rheology measurements and the temperature was controlled with a Peltier plate with circulating cooling liquid. The rheometer was brought to the desired temperature without pre-shearing.

2.13. Frequency sweep measurements

Initially oscillatory strain sweep tests at constant angular frequency in the range of 0.1–100 % strain were run to determine the viscoelastic region. Next, oscillatory frequency test was conducted by measuring storage (G') and loss (G'') moduli at the frequency between 0.1 and 150 rad/s.

3. Results and discussion

3.1. Characterizations of cellulose solutions prior to gelation

Stabilizing interactions in aqueous hydroxide cellulose solutions have been shown to be promoted by an increasing hydrophobicity of the cation leading to disruption of cellulose hydrophobic assembly (Swensson et al., 2020; Wang et al., 2018). Given the large hydrophobicity difference between the *N*-methylmorpholine and benzene (the n-octanol/water partition coefficient at 25 °C being −0.32 and 2.13 respectively (Sigma-Aldrich)) as well as the different alkyl chain length of the two studied morpholinium solvents, the studied solutions were expected to show an enhancing hydrophobicity effect on cellulose-solvent interactions when going from NDMMOH to BMMorOH and finally to Triton B, manifested as enhanced displacement of carbohydrate NMR-signals and a higher intrinsic viscosity of cellulose solutions. However, other structural differences among the studied cations should be kept in mind as influential in these interactions. Increased hydrophobicity of the cation was in the previous studies observed to displace the ^{1}H chemical shifts of the model methyl--α-D-glucopyranoside compound to higher ppm possibly indicating the displacement of the electron density away from the C—H protons due to the proximity of the cation (Swensson et al., 2020). At the same time, no effect on the level of deprotonation could be observed. In this study, thus, an analogous displacement (to higher ppm), i.e. an increasing deshielding of the glucose C—H moieties by the cation was expected when going from NDMMOH to BMMorOH and finally to TritonB. Interestingly, though, NMR measurements could not detect any substantial deviations in the chemical shifts of this model compound in the studied solvents (Fig. 1), indicating no significant differences in glucose-cation interactions that could be evident as shielding/deshielding effects. Just as in the previous study, no indications of changed level of deprotonation could be detected either (enhanced deprotonation of the cellulose hydroxyls has been associated with a downfield displacement of the ^{13}C and upfield displacement of ^{1}H chemical shifts as reported by Isogai (Isogai, 1997). The question is whether this similarity will be transferred to the rheological properties and response of the studied solutions to the CO_2-coagulation.

As expected, the solvents (in absence of MCC) showed low viscosity very close to water with a Newtonian behavior (Fig. 2a) appearing in the following order BMMorOH(aq) > Triton B(aq) > NDMMOH(aq). These viscosity differences are, though, not extended to the cellulose containing solutions, being significantly higher and very similar in BMMorOH(aq) and Triton B(aq) compared to NDMMOH(aq) (Fig. 2b). Yet, in all the three solvents the Newtonian behavior was preserved, indicating the stability of the solutions (absence of aggregates) while applying different shear rates. The obtained results reveal the differences in cellulose conformation and extension in different solvents and call for analysis of the intrinsic viscosity of cellulose in these systems, which would indicate the level of cellulose extension and provide a further insight in the observed viscosity differences.

Interestingly, despite the very similar dynamic viscosities observed during flow sweep measurements of cellulose solutions in Triton B(aq) and BMMorOH(aq), intrinsic viscosity values (Fig. 3) show a difference between these two solvents – 1.12 and 0.9 dL/g, respectively – indicating a slightly higher degree of cellulose extension in Triton B. The intrinsic viscosity of cellulose in NDMMOH(aq) was the lowest (0.78 dL/g) pointing out a lower polymer extension.

This interesting observation could point out a higher solvent quality of the Triton B with the more hydrophobic cation, despite the earlier anticipated favorable interactions of cellulose with the morpholinium based cations, making the investigation of the cellulose response in these solutions to CO_2-coagulation even more interesting.

3.2. In situ monitoring of cellulose gelation upon CO_2(g) introduction

For details on the reactions taking place in alkaline media when CO_2(g) is introduced into the system the reader is referred to the supporting materials. *In situ* FTIR monitoring of the precipitation process showed the expected occurrence and increase of the CO_3^{2-} signal upon addition of CO_2(g) accompanied with immediate decrease of the signals in the "cellulose region" (as a result of precipitation), followed by a decrease (due to its transformation into bicarbonates) and appearance of a bicarbonate characteristic peak (Fig. 4). For details on the reactions taking place in alkaline media when CO_2(g) is introduced into the system the reader is referred to the supporting materials.

Since the IR probe detects the dissolved state, it was expected that following the decrease in cellulose characteristic peaks during the coagulation would provide information on the duration of the process. Thus, attempts have been made to assess the time required for precipitation, as well as the extent of carbonate introduction during this process by following the decrease of the cellulose signals in relation to intensity of the carbonate absorption band. However, as solvent peaks overlap with cellulose characteristic peaks, both showing a decrease in absorbance during coagulation (the former due to water formation in the system via reaction between CO_2(g) and hydroxides) and the latter due to cellulose precipitation, a quantitative assessment of the precipitation was not possible. Attempts to subtract the solvent spectra from the corresponding spectra of the cellulose-containing systems were not successful either, since baseline shifts were observed due to unavoidable differences in probe alignment (angle).

However, a qualitative analysis of the carbonate, pH and temperature profiles during the coagulation was possible (Fig. 5). Interestingly, the three studied systems showed principally identical response to the CO_2-coagulation, as no significant deviations could be observed in pH, temperature, carbonate or bicarbonate species changes during the precipitation process.

Generally, as CO_2(g) is introduced into the solutions and carbonates are formed a sharp decrease in pH and increase in temperature is observed. Later, when carbonates reach their maximum and as a result of bicarbonate formation, the pH continuous to drop at a lower rate accompanied by a steady decrease in temperature.

In comparison to the cellulose-free solutions, a plateau in the CO_2(g) absorption of the cellulose containing solutions is indicative of the precipitation process. It is though unclear whether the rather constant level of the carbonate ion concentration during this stage originates from an equilibrium process or might be associated with the gelling preventing appropriate quantification by the FTIR probe.

3.3. Characterizations of cellulose systems after gelation

3.3.1. Rheological investigation

After addition of CO_2(g) and gelation of cellulose solutions, all the three samples showed shear thinning (pseudoplastic behavior with the viscosity decreased over increasing shear rates), typically observed for most of the gels (Fig. 6). Interestingly, the viscosity of the systems after gelation did not reflect the differences observed in the dissolved state

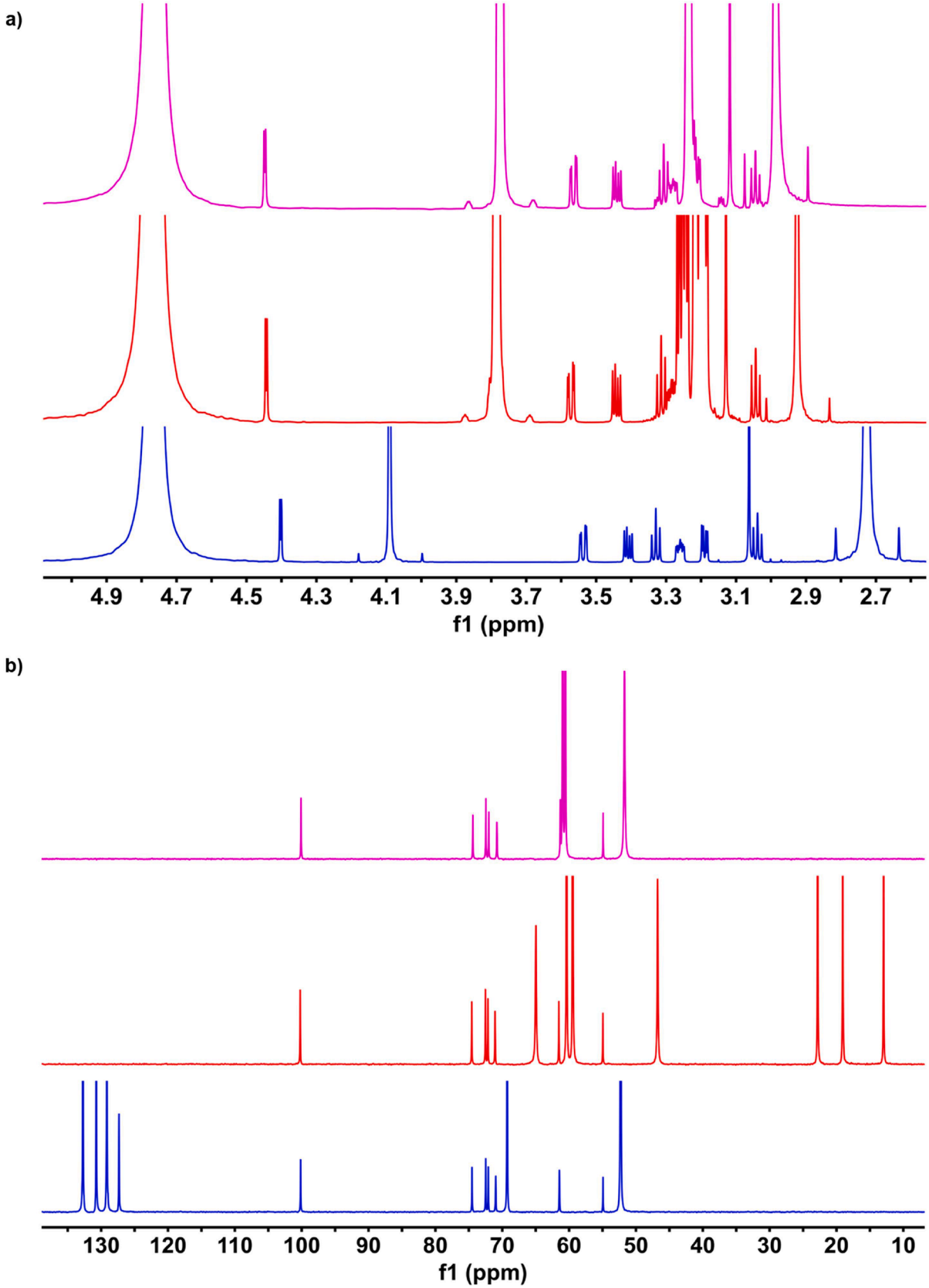

Fig. 1. a) ^{1}H NMR and b) ^{13}C NMR spectra of 3 wt% methyl-α-D-glucopyranoside as the model compound dissolved in 1.5 M NDMMOH(aq) (pink), 1.5 M BMMorOH (aq) (red) and 1.5 M Triton B(aq) (blue) in D_2O.

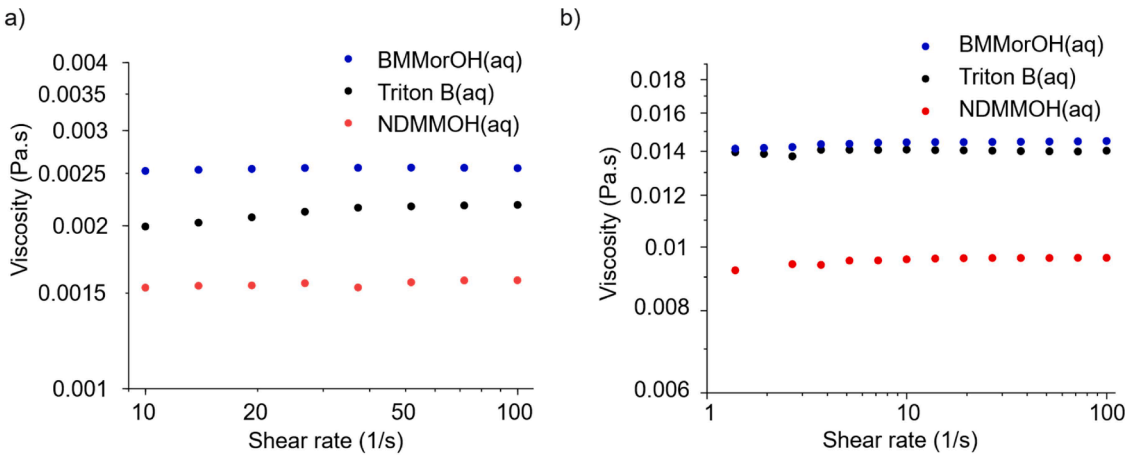

Fig. 2. Flow sweep curves of a) 1.5 M solvents b) 2 wt% MCC dissolved in 1.5 M solvents. Due to low viscosity of the solvents, flow responses < 10 l/s (in the measurements ran on only solvents) were noisy, thus not include.

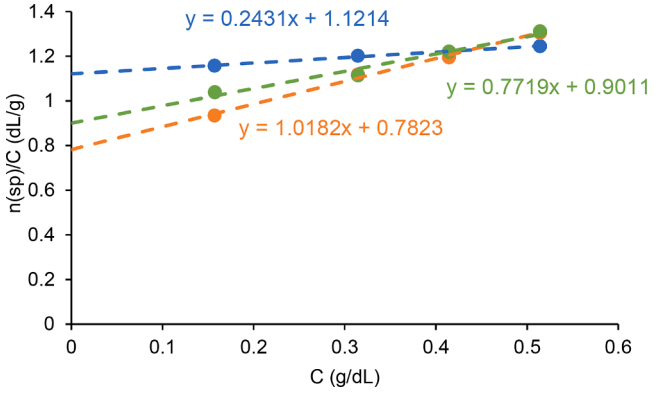

Fig. 3. Intrinsic viscosity extrapolated from and η_{sp} /C plotted vs. C in 1.5 M Triton B (blue), BMMorOH (green) and NDMMOH (orange).

(Fig. 2b): the remarkable viscosity deviation of the BMMorOH(aq) and Triton B(aq) from the NDMMOH(aq) system did not follow the same order after gelation. In fact, after gelation, the viscosity obtained in Triton B(aq) was significantly higher than that in BMMorOH(aq) as well as in NDMMOH(aq). These results were in agreement with what was visually observed during the gelation process where more compact (solid-like) gel was formed upon CO_2(g) introduction into Triton B(aq) while less compact gel was observed in BMMorOH(aq) and specially in NDMMOH(aq).

Indeed, the frequency sweep measurements yielding G' (solid contribution of the material) confirmed order of the obtained gels' strength: Triton B(aq) > BMMorOH(aq) > NDMMOH(aq) (Fig. 7b). In the obtained gels both G' and G'' were almost frequency independent, in contrast to frequency sweep measurements recorded on cellulose solutions before gelation (Fig. 7a).

3.3.2. *Crystallinity of the coagulated cellulose*

CP/MAS ^{13}C NMR characterization of the obtained gels revealed quite similar crystallinity of the gels obtained from NDMMOH(aq) and Triton B(aq) (compare the CO_2-coagulated gels in Fig. 8). However, when ethanol was used as a coagulant, for a comparison, the spectra showed a lower content of ordered material coagulate from Triton B (aq). The reference MCC spectrum (Fig. 8, pink) shows, peaks at 105.3 ppm (C1), 89 ppm (C4 crystalline), 84.3 ppm (C4 amorphous), 75.1 and 72.5 ppm (C2, C3 and C5), 65.3 ppm (C6 crystalline) and 63.1 ppm (C6 amorphous). Upon coagulation with either solvent, the absence of the peak at 65.3 corresponding to Cellulose I indicated no residual Cellulose I in any of the coagulated samples. The shift of the peak at 65.3 upfield in all of the samples indicates that the "*tg*" conformation of the C6–OH group for the crystalline cellulose I had changed into a "*gt*" or "*gg*" conformation of cellulose II or a less ordered material, respectively (Kamide et al., 1992; Li et al., 2012).

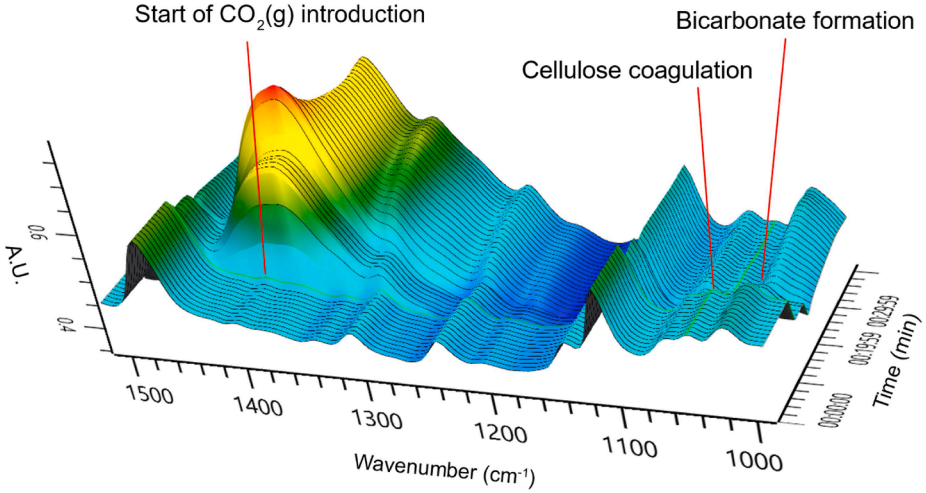

Fig. 4. 3D spectra of *in line* monitoring of cellulose gelation upon CO_2(g) introduction in NDMMOH(aq).

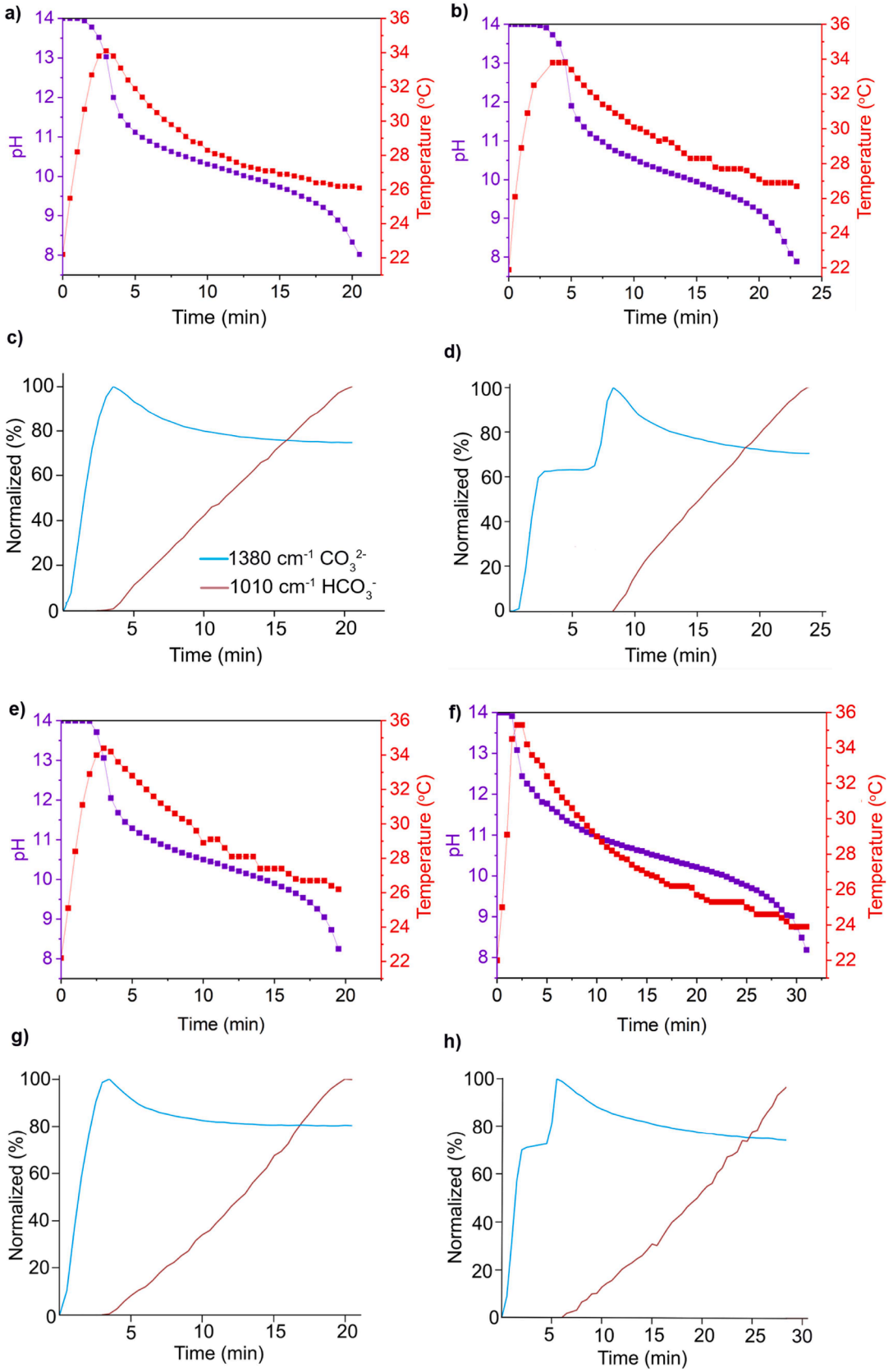

Fig. 5. pH, temperature and carbonate/bicarbonate trends (based on FTIR absorption), while introducing CO_2(g) (200 ml/min, room temperature) to the following solutions: a) & c) 1.5 M NDMMOH(aq); b) & d) 2 wt% MCC dissolved in 1.5 M NDMMOH(aq); e) & g) 1.5 M BMMorOH(aq); f) & h) 2 wt% MCC dissolved in 1.5 M BMMorOH (aq);) i) & k) 1.5 M Triton B(aq); j) & l) 2 wt% MCC in 1.5 M Triton B(aq).

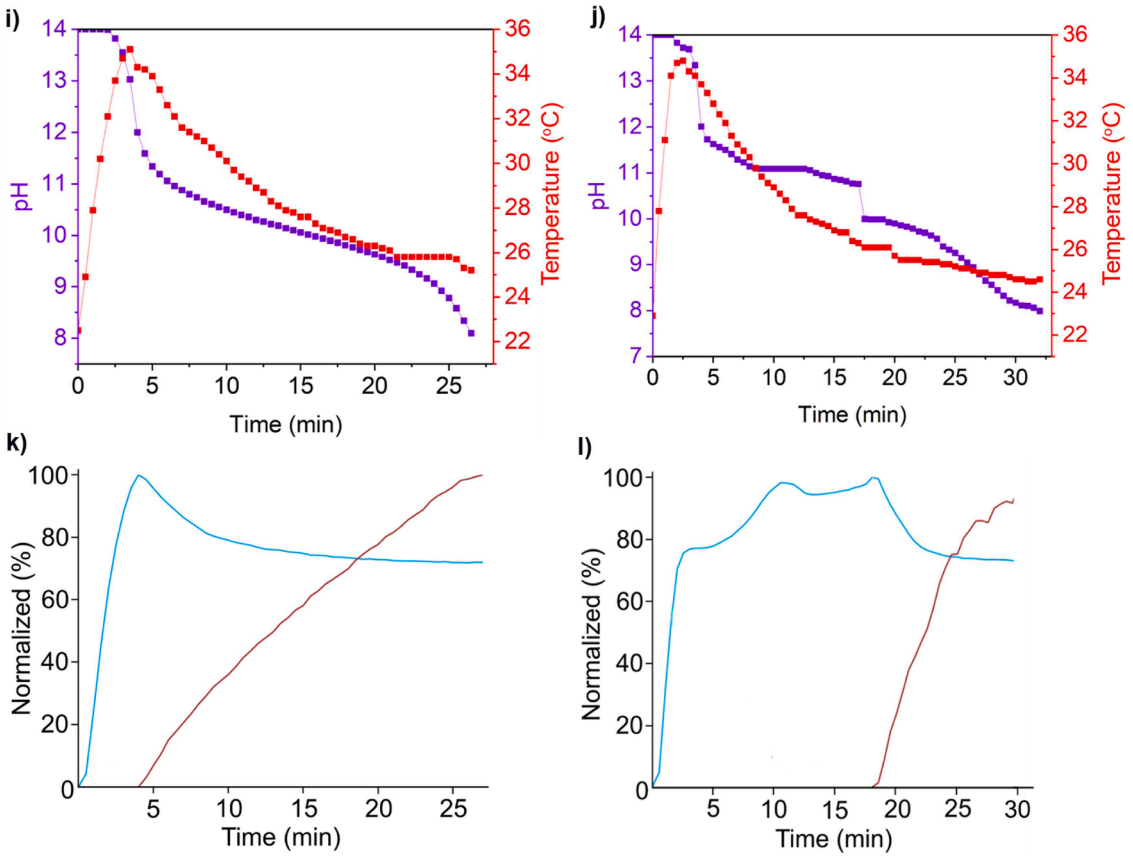

Fig. 5. (*continued*).

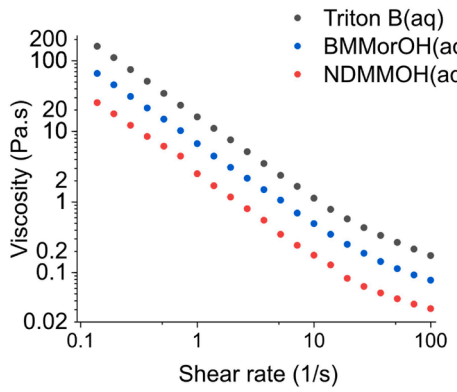

Fig. 6. Flow sweep curves of 2 wt% MCC dissolved in different solvents after CO_2(g) addition.

For samples coagulated in CO_2(g), appearance of the peak at 107.2 and 87.8 is characteristic of Cellulose II (Atalla et al., 1980; Idström et al., 2016; Lennholm & Iversen, 1995; Maciel et al., 1982; Zuckerstätter et al., 2009) and samples from both the solvents appear quite similar. On the other hand, when ethanol was used as the coagulant, cellulose regenerated from NDMMOH(aq) showed the peak at 87.8 ppm (cellulose II), while the peak at 107.2 was absent. Yet, for cellulose regenerated from Triton B none of the aforementioned peaks associated to cellulose II formation was detected, pointing out less ordered coagulated cellulose proven by peak at 83.6 ppm (non-ordered material).

Thus, coagulation using CO_2(g) seems to promote a higher crystallinity in the regenerated cellulose (both in NDMMOH(aq) and Triton B (aq)) while ethanol leads to more of the less ordered structure specially when Triton B is used as the solvent for cellulose. In the previous work (Naserifar et al., 2023), a slower diffusion of the solvent during coagulation was associated with formation of low-order regions. Similar results have been observed in studies where ethanol or water were used for coagulation of cellulose from EMIMAc. Those results have reported yielding more amorphous cellulose when using ethanol, while using water resulted in higher degree of cellulose II formation (Östlund et al., 2013; Tan et al., 2019). Östlund et al. explained the obtained lower crystallinity of ethanol-coagulated cellulose by a slower diffusion of EMIMAc in ethanol than in water.

3.3.3. *Complementary MD simulations*

The coagulated material from Triton B showed the highest gel strength despite the quite similar dynamic viscosity of the Triton B(aq) and BMMorOH(aq) solutions and similar level of stabilization through deprotonation and against CO_2-coagulation. At the same time, the longer alkyl chain of the BMMorOH(aq) seems to correlate with a higher dynamic viscosity of the solution, a higher level of polymer extension and a stronger gel (compared to the NDMMOH(aq)). To further elucidate the differences observed in the process of gel-like structure formation and the properties of the coagulated material, Molecular Dynamics (MD) simulations were performed (Angelerou et al., 2018; Jia et al., 2023). The calculated free energy profiles for interactions between the hydorophilic and hydrophobic faces in the studied solvents are depicted in Fig. 9a and b, respectively. The distance between the center of masses of cellulose chains is represenetd in X axis and potential of mean force (PMF) (attraction or repulsion) observed in the simulations is dispalyed on the y axis. In these MD simulations the Triton B(aq) cation is referred to as $BTMA^+$ (benzyltrimethylammonium cation) in the figures.

A system attains a stable state when it is encountered in the region of minimum energy (ROME). Energy maxima are present on both sides of the ROME. Therefore, the lower the ROME, the higher the force required

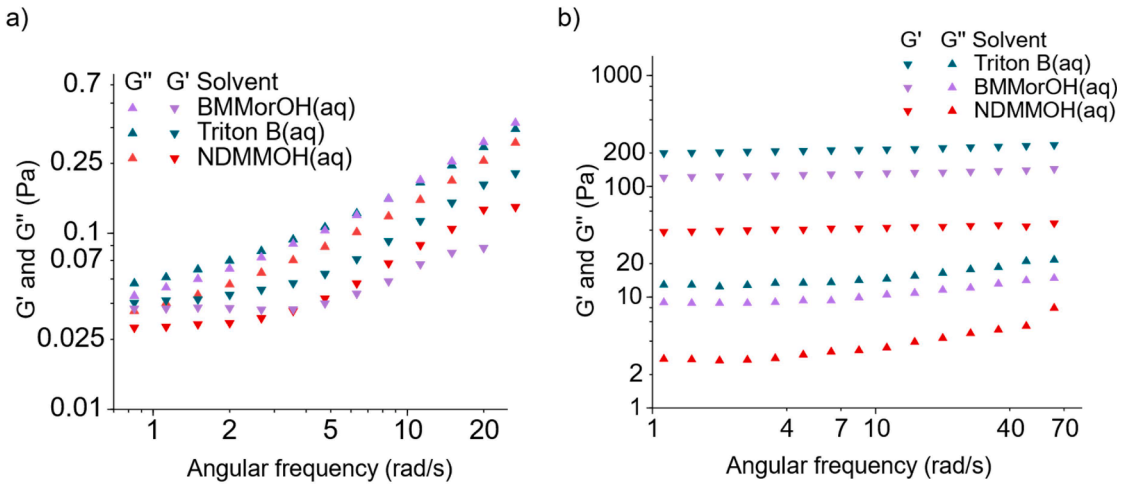

Fig. 7. Frequency sweep curves of 2 wt% cellulose dissolved in 1.5 M solvent a) before and b) after gelation.

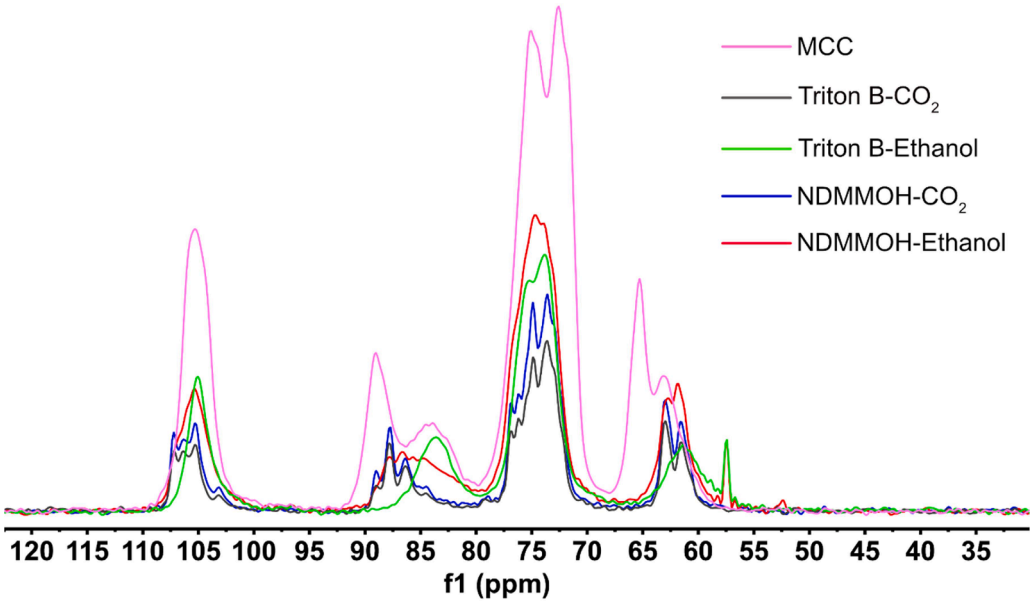

Fig. 8. CP/MAS ^{13}C NMR of reference cellulose and cellulose regenerated in different solvents by CO_2(g) vs. ethanol.

to separate the cellulose chains, resulting in a higher viscosity. Fig. 9a and b suggest that the systems are more likely to undergo a shift towards the right-hand side (RHS) when an external force is applied, due to the considerably lower energy barriers observed on RHS compared to those observed on the left-hand side (LHS). The specific depths and positions of these secondary minima depend on the solvents employed. It is evident from Fig. 9a (considering hydrophilic sides of cellulose prior to CO_2(g) introduction) that the chains tend to reside in the secondary energy minimum region (between 1.47 and 1.62 nm). Similar secondary minima is observed in the region between 1.0 and 1.62 nm when considering hydrophobic faces of the cellulose chains in the absence of carbonate ions (Fig. 9b). Comparing Fig. 9a and b indicates that energy barriers are more pronounced during interactions between the hydrophobic faces of the cellulose chains, pointing out that hydrophobic contributions play a more significant role in determining the viscosity of cellulose solutions. Considering this, the energy barriers that must be surpassed by cellulose chains considering hydrophobic faces of cellulose are quantitatively determined as follows: 2.5 kJ/mol for Triton B(aq), 2.4 kJ/mol for BMMorOH(aq), and 1.2 kJ/mol for NDMMOH(aq). This indicates that the viscosity of cellulose solution in Triton B(aq) should be similar to that of BMMorOH(aq), while the viscosity of NDMMOH(aq) is expected to be the lowest among the three solvents, which is in line with the experimantal results (compare Fig. 2).

To investigate the impact of introduced carbonate ions during coagulation, all the hydroxide ions were replaced with an equivalent number of carbonate ions. The charge neutrality of the suspension was maintained by adding additional positive counterions from the solvent. The free energy profiles of the cellulose-cellulose interactions, specifically between the hydrophobic and hydrophilic sides, in the presence of carbonate ions are presented in Fig. 10a and b, respectively. These figures illustrate that the presence of carbonate ions immediately generates a deep energy valley in all cases, with the interactions influenced most significantly by the hydrophobic component.

Analyzing Figs. 9b and 10b for the Triton B(aq), it appears that the carbonate ions have an immediate impact on creating a ROME (as seen between 1.0 and 1.8 nm). However, the position of the minimum valley shifts only slightly from its position. This observation is intriguing, as it predicts the instantaneous formation of a gel without the aggregation of cellulose chains. A similar behavior is observed in Triton B solutions containing carbonate ions. However, in the case of the NDMMOH(aq)

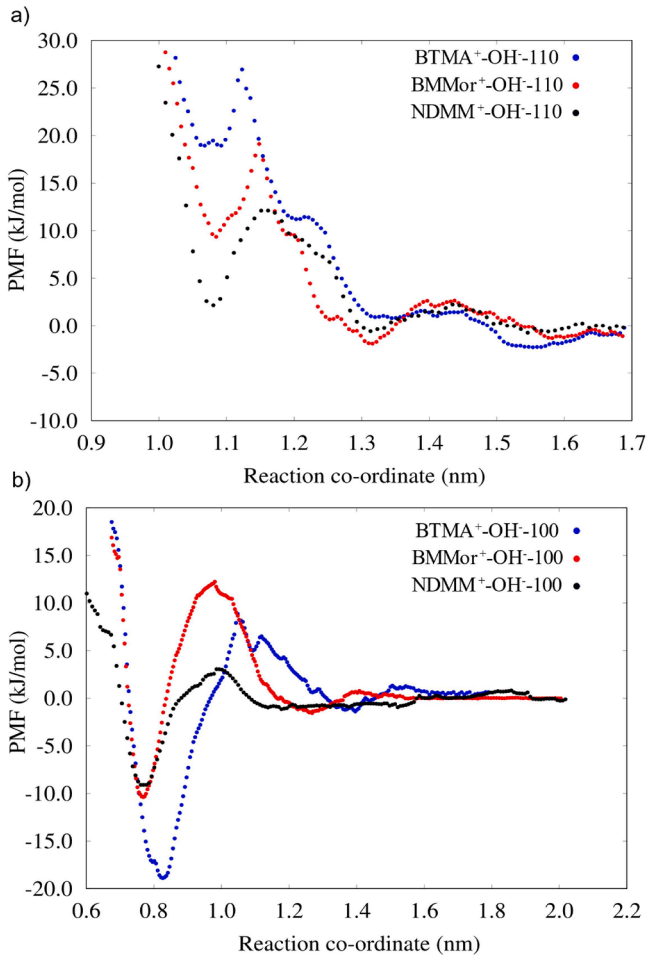

Fig. 9. a) Free energy profile of interaction between the hydrophilic (110–110) faces in presence of different solvents and OH^- ions, b) free energy profile of interaction between the hydrophobic (100–100) faces in presence of different solvents and OH^- ions. $BTMA^+$ refers to cation in Triton B(aq).

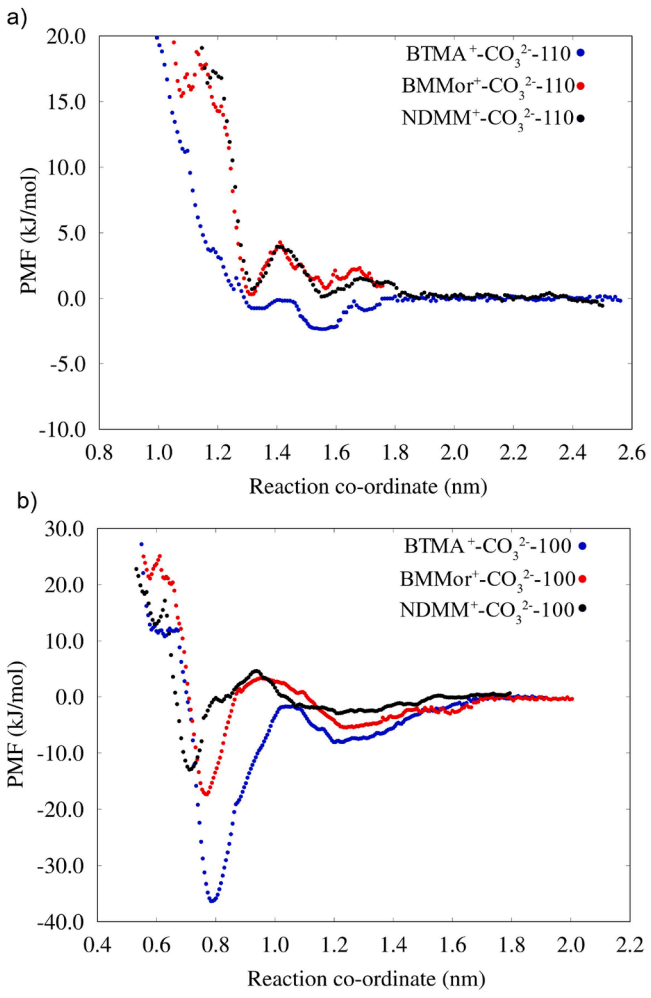

Fig. 10. a) Free energy profile of interaction between the hydrophilic (110–110) sides in presence of different solvents and CO_3^{2-} ions b) Free energy profile of interaction between the hydrophobic (100–100) sides in presence of different solvents and CO_3^{2-} ions. $BTMA^+$ refers to cation in Triton B(aq).

solvent, the ROME shifts further towards the RHS, indicating the expulsion of solvent molecules from between the cellulose chains and the formation of a loosely connected aggregate. In summary, the introduction of carbonate ions creates a deep energy minimum in the cellulose solutions, affecting the interactions primarily driven by the hydrophobic regions. The behavior differs slightly depending on the solvent used, with Triton B(aq) and BMMorOH(aq) solutions exhibiting immediate gel formation without significant chain aggregation (due to the creation of deep energy minima) while the NDMMOH(aq) shows a more pronounced shift in the valley position, suggesting the formation of a loose aggregate with expelled solvent molecules. The viscosity of the resulting gel is higher in the case of the Triton B(aq), while slightly lower in the case of the BMMorOH(aq) solution. Conversely, in the NDMMOH (aq) solution, very loose aggregates are formed, leading to the lowest viscosity in the suspension. Tendency of Triton B to remain associated to cellulose during coagulation might possibly also partly explain the lower order (crystallinity) of the material coagulated from Triton B when using ethanol (c.f. Fig. 8), considerig that a slower diffusion of the solvent during coagulation has been associated with formation of a less crystalline material. In the case of CO_2-coagulation, however, the hydrophobic pairing and the accompanying coagulation is possibly (in agreemennt with the observations above, Figs. 4. & 5.) sufficiently fast to promote formation of crystalline material. Tshis matter, howerver, requires further investigation.

4. Conclusions

The three studied hydroxide solvents varying in the structure of the cation showed clear differences in viscosity and coagulation behavior of their cellulose solutions, the could be correlated to their structural motifs capable of stabilizing dissolved cellulose against hydrophobic pairing. The intrinsic viscosity measurements indicated the highest expansion of cellulose chains in the most hydrophobic (i.e. benzyl substituted) Triton B, a trend that was valid for the two morpholinium solvents as well: a longer alkyl substituent of the cation correlated with a higher intrinsic viscosity of cellulose solutions. Consequently, the solvent with the poorest ability to interact with the more hydrophobic cellulose regions (NDMMOH(aq)) yielded cellulose solutions with a significantly lower dynamic viscosity compared to the other two (Triton B(aq) and BMMorOH(aq) showed higher and mutually very similar dynamic viscosities). Coagulation of cellulose from these solutions with CO_2(g) relied, as manifested by MD-simulations, on hydrophobic pairing and showed analogous dependency on the structural characteristics of the solvent: the presence of bulkier more hydrophobic substituents – a benzyl group in Triton B and a longer alkyl chain in BMMorOH – rendered formation of stronger gels involving also probably trapping of the solvent due to stronger cellulose-solvent interactions. Interestingly, these differences did not translate to any significant deviations in crystallinity between cellulose coagulated from NDMMOH(aq) and Triton B (aq), probably as coagulation with CO_2(g) is fast regardless of the

solvent system used promoting, thus, formation of crystalline material. On the other hand coagulation with ethanol yielded a less crystalline material from the Triton B (aq) solution (compared to the material obtained from the NDMMOH(aq) system), possibly due to stronger cellulose – Triton B interactions slowing down the coagulation process.

This study has been performed on three hydroxide solvents only and is not sufficient to draw general conclusions, but it clearly points out that the cation hydrophobicity likely promotes expansion of cellulose chains in the dissolved state, leading also to stronger gels upon coagulation, where the initial gelation might involve entrapping of the solvent (due to strong interactions with cellulose) rather than chain-chain aggregation. The level of order of the coagulated material depends strongly on the type of coagulant but might also be affected by the choice of solvent. Further work is needed to comprehensively elucidate the cellulose-solvent-coagulant interplay for tailoring of coagulated cellulose materials.

CRediT authorship contribution statement

Shirin Naserifar: Conceptualization, Methodology, Visualization, Investigation, Writing – original draft, Validation. **Nabin Kumar Karna:** Writing – review & editing, Methodology, Investigation, Conceptualization. **Aleksandra Maria Kozlowski:** Methodology, Writing – review & editing. **Diana Bernin:** Methodology, Investigation, Writing – review & editing. **Merima Hasani:** Conceptualization, Resources, Supervision, Writing – review & editing, Validation.

Declaration of competing interest

The authors declare that they have no known competing financial interests or personal relationships that could have appeared to influence the work reported in this paper.

Data availability

Data will be made available on request.

Acknowledgement

The Knut and Allice Wallenberg Foundation is gratefully acknowledged for financial support within Wallenberg Wood Science Center and the Swedish NMR Centre is acknowledged for providing spectrometer time. We also thank Tobias Sparrman at Umeå University for running solid state NMR. Professor Anna Ström is acknowledged for the access to the rheometer and Sylwia Wojno for rheology measurements discussions and Prof. Thomas Heinze's group for the provided chemicals used for the synthesis of the solevnts during the time of collaboration in Germany.

Supplementary materials

Supplementary material associated with this article can be found, in the online version, at doi:10.1016/j.carpta.2024.100514.

References

Angelerou, M. G. F., Frederix, P. W. J. M., Wallace, M., Yang, B., Rodger, A., Adams, D. J., Marlow, M., & Zelzer, M. (2018). Supramolecular nucleoside-based gel: Molecular dynamics simulation and characterization of its nanoarchitecture and self-assembly mechanism. *Langmuir : the ACS journal of surfaces and colloids, 34*(23), 6912–6921. https://doi.org/10.1021/acs.langmuir.8b00646

Atalla, R. H., Gast, J. C., Sindorf, D. W., Bartuska, V. J., & Maciel, G. E. (1980). Carbon-13 NMR spectra of cellulose polymorphs. *Journal of the American Chemical Society, 102*(9), 3249–3251. https://doi.org/10.1021/ja00529a063

Boerstoel, H., Maatman, H., Picken, S. J., Remmers, R., & Westerink, J. B. (2001). Liquid crystalline solutions of cellulose acetate in phosphoric acid. *Polymer, 42*(17), 7363–7369. https://doi.org/10.1016/S0032-3861(01)00209-9

Brownsett, T., & Clibbens, D. A. (1941). 4— The dissolution of chemically modified cotton cellulose in alklaline solutions. Part VII. The solevnt action of solutions of triemethylbenzyl-and dimethyldibenzyl- ammonium hydroxides (Tritons B and F). *Journal of the Textile Institute Transactions, 32*(2), T32–T44. https://doi.org/10.1080/19447024108659357

Clarence C. McCorsley, I. (1981). *Process for shaped cellulose article prepared from a solution containing cellulose dissolved in a tertiary amine N-oxide solvent* (Patent No. US4246221A).

Cross, C.F., Bevan, E.J., & Beadle, C. (1982). *Improvements in dissolving cellulose and allied compounds*. British patent 8.

Donald, E., & Reginald, W.W. (1951). *Production of viscose* (Patent No. US2542492A).

Ehert, R., & Lieser, V. T. (1937). Zur Eenntnis der Kohlenhydrate. X. *Viscositiitsuntersuchungen an Cellulose-Losungen, 532*, 94–103.

Ginsburg, D. (1967). Properties, preparation and reactions. *Concerning amines* (p. 75). Elsevier Ltd. https://doi.org/10.1016/b978-0-08-011913-7.50014-8

Gubitosi, M., Duarte, H., Gentile, L., Olsson, U., & Medronho, B. (2016). On cellulose dissolution and aggregation in aqueous tetrabutylammonium hydroxide. *Biomacromolecules, 17*, 2873–2881. https://doi.org/10.1021/acs.biomac.6b00696. *2016*.

Idström, A., Schantz, S., Sundberg, J., Chmelka, B. F., Gatenholm, P., & Nordstierna, L. (2016). C NMR assignments of regenerated cellulose from solid-state 2D NMR spectroscopy. *Carbohydrate Polymers, 151*, 480–487. https://doi.org/10.1016/j.carbpol.2016.05.107

Isogai, A. (1997). NMR analysis of cellulose dissolved in aqueous NaOH solutions. *Cellulose (London, England), 4*(2), 99–107. https://doi.org/10.1023/A:1018471419692

Jia, X., Chen, J., Xu, W., Wang, Q., Wei, X., Ma, Y., & Zhang, G. (2023). Molecular dynamics study of low molecular weight gel forming salt-triggered dipeptide. *Scientific Reports, 13*(1), 6328. https://doi.org/10.1038/s41598-023-33166-3

Kamide, K., Okajima, K., & Kowsaka, K. (1992). Dissolution of natural cellulose into aqueous alkali solution: Role of super-molecular structure of cellulose. *Polymer Journal, 24*(1), 71–86. https://doi.org/10.1295/polymj.24.71

Kostag, M., Jedvert, K., Achtel, C., Heinze, T., & El Seoud, O. A. (2018). Recent advances in solvents for the dissolution, shaping and derivatization of cellulose: Quaternary ammonium electrolytes and their solutions in water and molecular solvents. *Molecules (Basel, Switzerland), 23*(3). https://doi.org/10.3390/molecules23030511

Lennholm, H., & Iversen, T. (1995). Estimation of cellulose I and II in cellulosic samples by principal component analysis of 13C-CP/MAS-NMR-spectra. *Holzforschung, 49*(2), 119–126. https://doi.org/10.1515/hfsg.1995.49.2.119

Li, R., Zhang, L., & Xu, M. (2012). Novel regenerated cellulose films prepared by coagulating with water: Structure and properties. *Carbohydrate Polymers, 87*(1), 95–100. https://doi.org/10.1016/j.carbpol.2011.07.023

Liebert, T. F., & Heinze, T. J. (2001). Exploitation of reactivity and selectivity in cellulose functionalization using unconventional media for the design of products showing new superstructures. *Biomacromolecules, 2*, 1124–1132. https://doi.org/10.1021/bm010068m

Lilienfeld, L. (1930). *Cellulose solutions and process for their production* (Patent No. US1771462A).

Maciel, G. E., Kolodziejski, W. L., Bertran, M. S., & Dale, B. E. (1982). Carbon-13 NMR and order in cellulose. *Macromolecules, 15*(2), 686–687. https://doi.org/10.1021/ma00230a097

Mccormick, C. L., Callais, P. A., & Hutchinson, B. H. (1985). Solution studies of cellulose in lithium chloride and N,N-dimethylacetamide. *Macromolecules, 7*, 2394–2401.

Medronho, B., & Lindman, B. (2015). Brief overview on cellulose dissolution/regeneration interactions and mechanisms. *Advances in Colloid and Interface Science, 222*, 502–508. https://doi.org/10.1016/j.cis.2014.05.004

Naserifar, S., Koschella, A., Heinze, T., Bernin, D., & Hasani, M. (2023). Investigation of cellulose dissolution in morpholinium-based solvents: Impact of solvent structural features on cellulose dissolution. *RSC Advances, 13*(27), 18639–18650. https://doi.org/10.1039/D3RA03370H

Naserifar, S., Swensson, B., Bernin, D., & Hasani, M. (2021). Aqueous N,N-dimethylmorpholinium hydroxide as a novel solvent for cellulose. *European Polymer Journal, 161*(September), Article 110822. https://doi.org/10.1016/j.eurpolymj.2021.110822

Olsson, C., & Westman, G. (2013). Direct dissolution of cellulose: Background, means and applications. *Cellulose - Fundamental Aspects* (pp. 2–37). Intech. https://doi.org/10.5772/52144

Östlund, Å., Idström, A., Olsson, C., Larsson, P. T., & Nordstierna, L. (2013). Modification of crystallinity and pore size distribution in coagulated cellulose films. *Cellulose (London, England), 20*(4), 1657–1667. https://doi.org/10.1007/s10570-013-9982-7

O'sullivan, A. C. (1997). Cellulose: The structure slowly unravels. *Cellulose (London, England), 4*(3), 173–207. https://doi.org/10.1023/A:1018431705579

Powers, D.H., & Bock, L.H. (1935). *Cellulose Solutions* (Patent No. US2009015A).

Sigma-Aldrich. (n.d.). https://www.sigmaaldrich.com.

Swensson, B., Larsson, A., & Hasani, M. (2020). Dissolution of cellulose using a combination of hydroxide bases in aqueous solution. *Cellulose (London, England), 27*(1), 101–112. https://doi.org/10.1007/s10570-019-02780-8

Tan, X., Chen, L., Li, X., & Xie, F. (2019). Effect of anti-solvents on the characteristics of regenerated cellulose from 1-ethyl-3-methylimidazolium acetate ionic liquid. *International Journal of Biological Macromolecules, 124*, 314–320. https://doi.org/10.1016/j.ijbiomac.2018.11.138

Wang, Y., Liu, L., Chen, P., Zhang, L., & Lu, A. (2018). Cationic hydrophobicity promotes dissolution freezing – thawing. *Physical Chemistry Chemical Physics, 20*, 14223–14233. https://doi.org/10.1039/c8cp01268g

Wei, W., Wei, X., Gou, G., Jiang, M., Xu, X., Wang, Y., Hui, D., & Zhou, Z. (2015). Improved dissolution of cellulose in quaternary ammonium hydroxide by adjusting temperature. *RSC Advances, 5*(49), 39080–39083. https://doi.org/10.1039/c5ra04247j

Xia, Y., Moran, S., Nikonowicz, E. P., & Gao, X. (2008). Z-restored spin-echo 13C 1D spectrum of straight baseline free of hump, dip and roll. *Magnetic Resonance in Chemistry, 46*(5), 432–435. https://doi.org/10.1002/mrc.2195

Zhong, C., Wang, C., Wang, F., Jia, H., Wei, P., & Zhao, Y. (2015). Application of tetra-n-methylammonium hydroxide on cellulose dissolution and isolation from sugarcane bagasse. *Carbohydrate Polymers, 136*, 979–987. https://doi.org/10.1016/j.carbpol.2015.10.001

Zhu, S., Wu, Y., Chen, Q., Yu, Z., Wang, C., Jin, S., Ding, Y., & Wu, G. (2006). Dissolution of cellulose with ionic liquids and its application: A mini-review. *Green Chemistry, 8*(4), 325–327. https://doi.org/10.1039/b601395c

Zuckerstätter, G., Schild, G., Wollboldt, P., Röder, T., Hedda, K., & Sixta, H. (2009). The elucidation of cellulose supramolecular structure by 13C CP-MAS NMR. *Lenzinger Berichte, 87*, 38–46.